Influence of tides on melting and freezing beneath Filchner-Ronne Ice Shelf, Antarctica

Keith Makinson,[1] Paul R. Holland,[1] Adrian Jenkins,[1] Keith W. Nicholls,[1] and David M. Holland[2]

Received 10 December 2010; revised 24 January 2011; accepted 3 February 2011; published 16 March 2011.

[1] An isopycnic coordinate ocean circulation model is applied to the ocean cavity beneath Filchner-Ronne Ice Shelf, investigating the role of tides on sub-ice shelf circulation and ice shelf basal mass balance. Including tidal forcing causes a significant intensification in the sub-ice shelf circulation, with an increase in melting (3-fold) and refreezing (6-fold); the net melt rate and seawater flux through the cavity approximately doubles. With tidal forcing, the spatial pattern and magnitude of basal melting and freezing generally match observations. The 0.22 m a^{-1} net melt rate is close to satellite-derived estimates and at the lower end of oceanographic values. The Ice Shelf Water outflow mixes with shelf waters, forming a cold (<−1.9°C), dense overflow (0.83 Sv) that spills down the continental slope. These results demonstrate that tidal forcing is fundamental to both ice shelf-ocean interactions and deep-water formation in the southern Weddell Sea.
Citation: Makinson, K., P. R. Holland, A. Jenkins, K. W. Nicholls, and D. M. Holland (2011), Influence of tides on melting and freezing beneath Filchner-Ronne Ice Shelf, Antarctica, *Geophys. Res. Lett.*, *38*, L06601, doi:10.1029/2010GL046462.

1. Introduction

[2] Processes over the Southern Weddell Sea and beneath Filchner-Ronne Ice Shelf (FRIS) convert shelf waters into cold dense water masses that flow down the continental slope into the abyss [*Foldvik et al.*, 2004] (Figure 1a). Brine rejection during intense wintertime sea ice formation generates cold (~−1.9°C), dense High Salinity Shelf Water (HSSW), some of which drains beneath FRIS to the deep grounding lines where the ice sheet first goes afloat. With the melting point depressed by the high pressure, rapid melting occurs, generating fresher buoyant Ice Shelf Water (ISW). As it ascends the sloping ice shelf base, the in situ pressure freezing point increases and the ISW becomes super-cooled, causing freezing and the formation of extensive accumulations of basal marine ice up to 400 m thick [*Lambrecht et al.*, 2007] (Figure 1b). The associated brine rejection creates a downwards flow that in turn leads to further melting at depth, creating a self-sustaining overturning circulation or 'ice pump', effectively redistributing ice from thicker to thinner parts of the ice shelf [*Lewis and Perkin*, 1986]. The processes of basal melting and freezing not only yield outflowing ISW with temperatures as low as −2.3°C [*Gammelsrød et al.*, 1994] but also shape the geometry of FRIS [*Lambrecht et al.*, 2007] and modify its rheology [*Larour et al.*, 2005], factors that have a significant influence on the flow of both ice shelf and ice sheet. ISW exiting FRIS escapes Filchner Depression and spills down the continental slope (Figure 1a), mixing with the overlying Weddell Deep Water to form Weddell Sea Bottom Water. Sub-ice shelf processes therefore play a role in both the properties and flux of deep ocean water masses, and the mass budget of the Antarctic Ice Sheet.

[3] Direct oceanographic observations from FRIS and the southern Weddell Sea have revealed several aspects of the sub-ice shelf circulation [*Nicholls et al.*, 2009] (Figure 1a) and yielded estimates of the freshwater flux out of the cavity. In estimating the net melt water input beneath FRIS, tracers such as oxygen isotopes and temperature give an average basal melt rate ranging from 0.20 to 0.34 m a^{-1} [*Nicholls et al.*, 2009]. Using satellite-derived ice velocities combined with ice thickness and snow accumulation data, and assuming steady state, *Joughin and Padman* [2003] estimated a net basal melt rate of 0.20 ± 0.06 m a^{-1}.

[4] Previous ocean modeling has considered many aspects of the circulation beneath FRIS, such as buoyancy forcing [e.g., *Jenkins and Holland*, 2002; *Timmermann et al.*, 2002], seasonal forcing [*Jenkins et al.*, 2004], barotropic and baroclinic tidal currents [e.g., *Robertson*, 2005], tidal mixing and residual currents [*MacAyeal*, 1984; *Makinson and Nicholls*, 1999], and ISW plumes [*Holland et al.*, 2007]. However, no study has yet combined sub-ice shelf ocean circulation with tidal forcing. In a region such as FRIS, where the buoyancy-driven circulation is significantly weaker than typical tidal currents, tides are likely to have a profound effect. Using a numerical ocean model, this study for the first time investigates the role of tidal forcing in melting and freezing processes beneath FRIS, its impact on sub-ice shelf circulation and its contribution to deep and bottom water formation.

2. Model

[5] We use a version of the Miami Isopycnic Coordinate Ocean Model [*Bleck et al.*, 1992] adapted to include sub-ice shelf cavities, because its evolving vertical coordinate allows a natural implementation of both the ice shelf and the tidal forcing on the ocean free surface [*Holland and Jenkins*, 2001]. The model domain encompasses the southern Weddell Sea continental shelf between 85°W and 28°W, and 71°S and 84°S, including that covered by FRIS (Figure 1a) and is discretized using an isotropic grid with a horizontal resolution ranging from 4.5 km in the south to 12.5 km in the

[1]British Antarctic Survey, Cambridge, UK.
[2]Courant Institute of Mathematical Sciences, New York University, New York, New York, USA.

0094-8276/11/2010GL046462

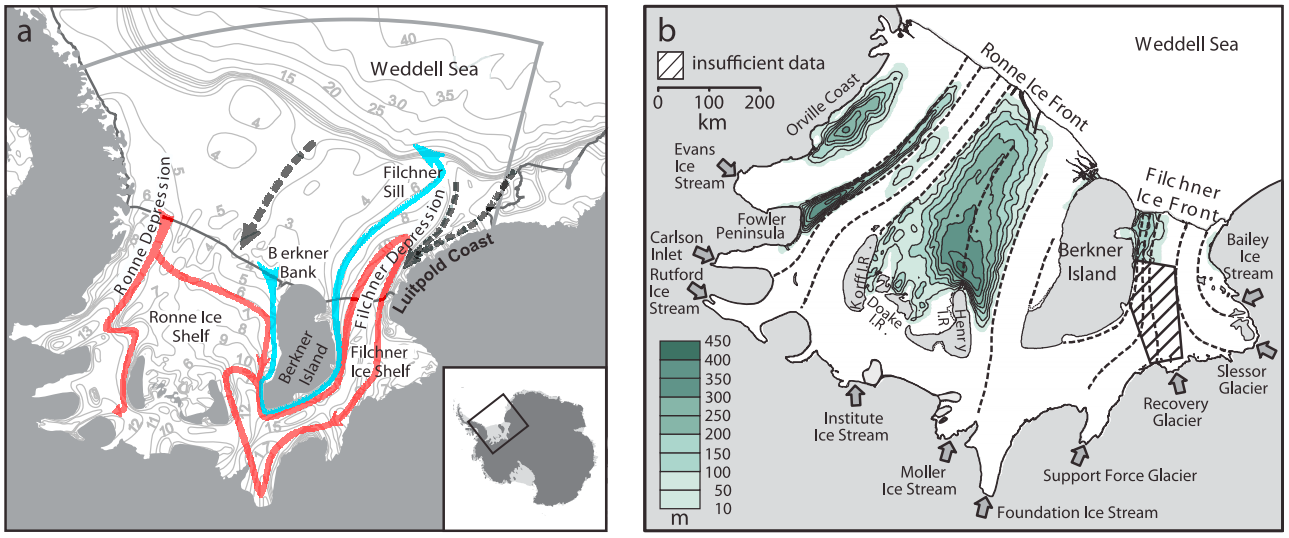

Figure 1. (a) Map of the southern Weddell Sea and FRIS, showing the northern and eastern model domain boundary (thick grey line) and the ice fronts (black lines). The contours are isobaths labeled in hundreds of meters. The broad arrows show the principal ocean circulation inferred from oceanographic observations [after *Nicholls et al.*, 2009]. (b) Basal marine ice thickness beneath FRIS [after *Lambrecht et al.*, 2007].

north. The ocean comprises 15 isopycnic layers and a surface mixed layer with a freely evolving density. The model bathymetry uses data from BEDMAP [*Lythe and Vaughan*, 2001] and the elevation of the ice base is from *Lambrecht et al.* [2007].

[6] We include neither wind forcing nor a sea ice model. We instead follow *Jenkins et al.* [2004] in restoring the surface salinity over the open ocean to a seasonally-varying field with a 15-day relaxation time period. An annual cycle approximating the growth and decay of sea ice is generated by ramping up [down] the surface salinities by 0.3 over a 3-month period beginning in mid-March [-September] while the temperature is maintained at the surface freezing point throughout. The peak wintertime salinity pattern is based on summertime bottom salinities [*Gammelsrød et al.*, 1994; *Nicholls et al.*, 2003] and winter observations from tagged Weddell Seals [*Nicholls et al.*, 2008], with the salinity of the continental shelf waters broadly increasing to the south and west.

[7] Initial ocean conditions are derived from *Olbers et al.* [1992]. These data also provide the northern and eastern boundary conditions, applied throughout the simulations by relaxation of the outer five rows of grid cells using baroclinic-restoring timescales of 10–30 days. In the second model simulation, surface elevations at these boundaries are restored (with 1–3 minute timescales) to those predicted by the Circum-Antarctic Tidal Simulation (CATS) [*Padman et al.*, 2002] utilizing 10 tidal constituents. The walls act as no-slip closed boundaries while the seabed and ice shelf basal drag use a quadratic law with a coefficient of 0.0025. With an 11.7-second time step, the model is run with and without tidal forcing for 20 years and the final year's averaged results from each simulation will now be discussed.

3. Results

[8] In both simulations the general pattern of circulation and water mass properties over the open continental shelf are broadly consistent with the sparse observations [e.g., *Gammelsrød et al.*, 1994; *Nicholls et al.*, 2003], and therefore provide a realistic northern boundary for the FRIS cavity. The highest salinity waters (34.81) are within Ronne Depression, followed by those on Berkner Bank (34.74). Lower salinity waters (34.55–34.3) are associated with the continental slope, the trough linking the shelf break to the central Ronne Ice Front region, and the Luitpold Coast. Along Ronne Ice Front the flow is from east to west, with the primary HSSW inflow in Ronne Depression (Figure 2). Other smaller inflows occur at the eastern corners of Ronne and Filchner ice fronts. Within the cavity, there are a number of internal gyres but the large-scale circulation is from west to east via the deep southern troughs. However, the model does not show the extensive recirculation within Filchner Depression suggested by *Nicholls et al.* [2009] (Figure 1a) and *Timmermann et al.* [2002]; rather the flow is almost entirely to the northeast at all levels, towards Filchner Ice Front (Figure 2).

[9] When forced with tides, the sub-ice shelf turbulent kinetic energy production increases by 3 to 4 orders of magnitude in the thin water column region along Ronne Ice Front, reaching 1 W m^{-2} and fully mixing the water column. This mixed zone prevents HSSW flowing deep into the cavity (Figure 2c) by transforming it into buoyant ISW that is returned to the along-ice front flow (Figure 2d). However, close to Berkner Island a small inflow of HSSW (Table 1) penetrates deeper into the cavity (Figure 2d). In the tidal case, the only inflow of unmodified HSSW occurs at the western side of Ronne Depression (Figure 2c) and is 63% greater than without tides (Table 1). Close to the ice front, the melt associated with these two inflows with tidal forcing is 2–3 m a^{-1}, significantly higher than without tidal forcing (Figure 3). The only other inflow occurs at the eastern Filchner Ice Front as part of a localized recirculation, and has an associated melt rate of 1 m a^{-1}. Tidal amplitudes within the domain are 15% smaller than predicted by CATS

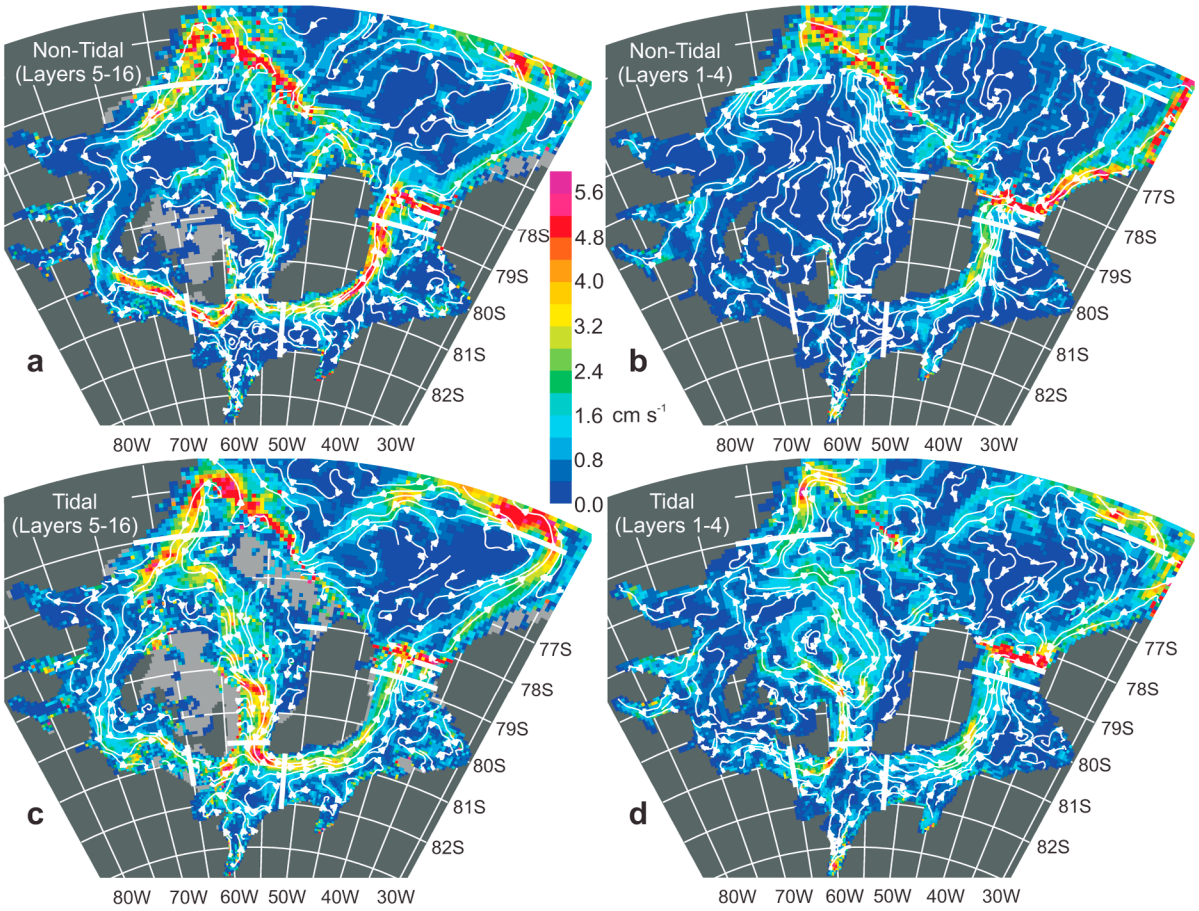

Figure 2. Flow lines of the modeled mean annual circulation in (a) the lower twelve layers without tides, (b) the upper four layers (including the mixed layer) without tides, (c) the lower twelve layers with tides, and (d) the upper four layers with tides. The black shading is land, the grey shading is where those layers have no volume. The color scale shows the mean current speed. The thick white lines are the flux gate locations listed in Table 1.

at the southern grounding lines, with the mis-match decreasing to zero at the restoring boundaries.

[10] Once beneath Ronne Ice Shelf, the ridge on the eastern side of Ronne Depression supports a rotationally trapped dense HSSW downslope flow; when its maximum geostrophic downslope transport is exceeded, the flow divides as the excess spills over the ridge to the southeast (Figure 2c). The densest HSSW remains trapped by the ridge on the western side of the Ronne cavity, while the less dense HSSW flows southeast, with both flows finally pooling in the deepest parts of the cavity.

[11] The arrival of these relatively warm waters at the grounding lines, coupled with steep basal slopes, drives strong basal melting. With tides, peak melt rates in the ice stream embayments are 5.5 m a^{-1} (Evans), 8.5 m a^{-1} (Carlson), 3.5 m a^{-1} (Rutford), 9 m a^{-1} (Institute), 1 m a^{-1} (Möller), 18 m a^{-1} (Foundation), and 2.5–4 m a^{-1} for ice streams entering Filchner Ice Shelf, approximately 1.3 to 8 times greater than without tides (Figures 3a and 3c). One other notable region of high melt occurs south of Henry Ice Rise, where the tidal case gives rates of up to 7 m a^{-1} and an area average of 1.85 m a^{-1}, compared with only 0.02 m a^{-1} without tides.

[12] Under the influence of rotation, the resulting buoyant ISW gathers along western coastlines (Figure 2c) where reducing ambient pressures cause supercooling and basal freezing (Figure 3c). With tides, peak freezing rates along Orville Coast and Fowler Peninsula (1.4 m a^{-1}), western Filchner Ice Shelf (1.1 m a^{-1}), central Ronne Ice Shelf (2.5 m a^{-1}), and between Doake Ice Rumples (1.3 m a^{-1}) are 3 to 10 times greater than without tides (Figure 3).

[13] There are similarities in the melt/freeze pattern predicted by the tidal and non-tidal cases (Figures 3b and 3c), but the absolute magnitudes differ markedly, with the magnitude of freezing showing a 6-fold increase on average with tides. The additional net flux through the cavity and intensified internal recirculation, driven by tidal mixing, results in the transport of 69 Gt a^{-1} of ice from deep to shallower regions (Table 2). With tidal forcing, the spatial pattern and magnitude of basal melting and freezing in Figure 3c reproduces almost all the major observed features [*Joughin and Padman*, 2003] (Figure 3d). The average net melt rate is 0.22 m a^{-1}, which is a doubling over the non-tidal case (Table 2); close to satellite-derived observations, but still at the lower end of estimates from oceanographic observations [*Nicholls et al.*, 2009] and models that parameterize tidal activity [e.g., *Timmermann et al.*, 2002].

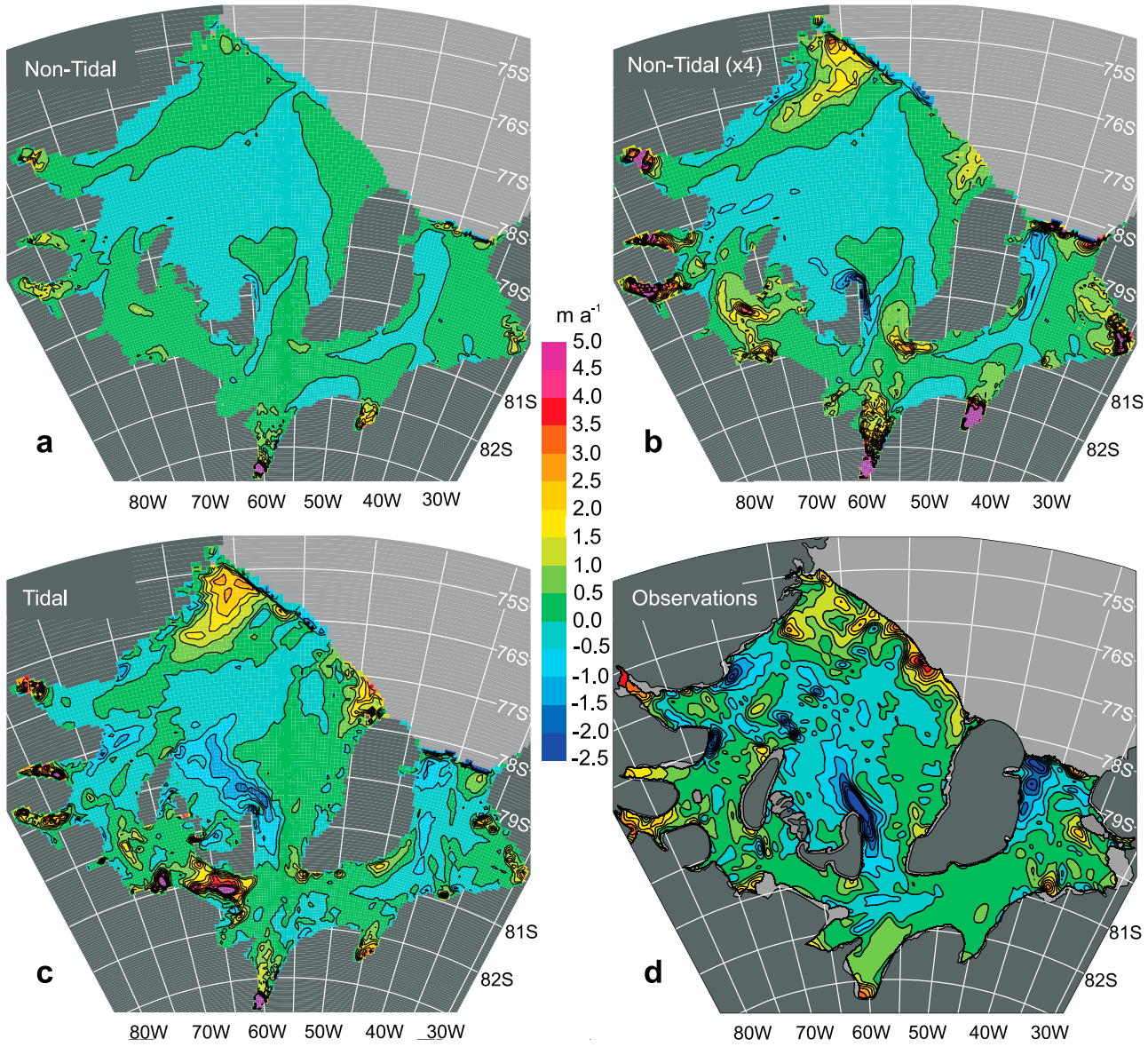

Figure 3. Mean basal ice melt rates beneath FRIS in cm a^{-1} from the model for (a) non-tidal, (b) non-tidal amplified by four to highlight melt rate details, and (c) tidal simulations. (d) The satellite-derived basal melt rates assuming steady state [after *Joughin and Padman*, 2003]. Negative values indicate freezing.

[14] Outflows of ISW occur around the central Ronne Ice Front and within Ronne Depression, but these remain close to the ice front before re-entering the cavity (Figures 2b and 2d), in agreement with observations [*Nicholls et al.*, 2003]. The only outflow of ISW that crosses the continental shelf to reach the shelf break lies within Filchner Depression (Figures 2a and 2c). Beneath FIS, the 0.58 Sv northward ISW flow and the southerly Luitpold Coast flow converge at Filchner Ice Front. Vigorous mixing and melting in this eastern ice front convergence zone enables 0.83 Sv of ISW

Table 1. Net Mean Annual Ocean Fluxes Through the Gates in Figure 2

Flux Gate	Non-tidal (Sv)	Tidal (Sv)
Ronne Depression (76°S)	0.38	0.62
Eastern Ronne Inflow (78°S)	0.05	0.03
East Henry Ice Rise (80.7°S)	0.12	0.41
South Henry Ice Rise (65°W)	0.21	0.17
Filchner Depression (53°W & 78.8°S)	0.32	0.58
Eastern Filchner Ice Front (78.4°S)	0.36	0.40
Filchner Sill (75°S) (<1.9°C)	0.46	0.83

Table 2. FRIS Mean Annual Basal Melt/Freeze Rates

	Non-tidal m a^{-1} (Gt a^{-1})	Tidal m a^{-1} (Gt a^{-1})	JP03[a] Gt a^{-1}
Melt	0.128 (53)	0.383 (160)	152
Freeze	0.028 (12)	0.165 (69)	73
Net melt	0.098 (41)	0.220 (92)	79 (83.4 ± 24.8)[b]

[a]From *Joughin and Padman* [2003] using flux gate divergence.
[b]Alternatively using ice shelf velocity, thickness and surface accumulation.

(<−1.9°C) to gain sufficient buoyancy to escape the depression via the Filchner Sill, a 80% higher flux than in the non-tidal case (Table 1).

4. Discussion

[15] Although the results from our ocean circulation model do not match all of the observational details, most of the key features become established when tidal forcing is applied. The distribution and magnitude of melting and freezing agree remarkably well with the observations of *Joughin and Padman* [2003] (Figure 3d) and with the accumulation zones implied by the marine ice bodies within FRIS [*Lambrecht et al.*, 2007] (Figure 1b). Unlike previous circulation models [e.g., *Jenkins and Holland*, 2002] the extensive ice front melting is reproduced, except for the region of highest melt around 53°W (Figure 3d) where Modified Warm Deep Water (MWDW) flows beneath FRIS [*Foldvik et al.*, 2001]. This flow across the open shelf is neither sufficiently warm nor well developed within the model to cause vigorous melting at this location, allowing the central RIS freezing region to extend to the ice front. However, ISW exiting the cavity around 55°W agrees with ice front observations [*Gammelsrød et al.*, 1994]. These results suggest that converging MWDW, ISW and HSSW mix in this central ice front region, forming a water mass that enters the cavity further west.

[16] Melt rates are anomalously high in the region south of Henry Ice Rise for the tidal case, averaging 1.85 m a^{-1} and exceeding 5 m a^{-1} in some places (Figure 3c), compared with only 0.02 m a^{-1} for the non-tidal case (Figure 3b), while *Joughin and Padman* [2003] show melting of around 0.4 m a^{-1} (Figure 3d). The modeled flow into the region west of Korff Ice Rise is almost 50% greater and 0.03–0.13°C warmer in the tidal simulation than observed by *Nicholls and Makinson* [1998]. The retention of heat in the deepest model layers, which result from a lack of diapycnal mixing within the model, appears, therefore, to be responsible for the high melt rates south of Henry Ice Rise. Furthermore, in the tidal case, the 2–3 cm s^{-1} eastward flow south of Henry Ice Rise becomes the main source of ISW for the central RIS freezing region, preventing ISW from the embayments of Foundation and Möller ice streams turning west under rotation (Figures 2b and 2d). This was a key problem encountered by the 2-D model of *Holland et al.* [2007], which was unable to reproduce the central RIS freezing area. Only about one third of ISW from the Foundation Ice Stream embayment flows northward, with the remainder flowing east beneath FIS.

[17] At the FRIS ice front, the water column thickness reduces by 25–75%, creating a significant dynamic barrier to flow into the cavity. The inclusion of tides boosts the Ronne Depression inflow from 0.38 Sv to 0.62 Sv (Table 1), as semi-diurnal tides with excursions of up to 5–7 km advect relatively warm water beneath the ice front. This advection induces melting and thus detrainment from the mixed layer, fuelling the deepest layers. Ultimately, this inflow emerges from Filchner Ice Front, where further mixing (with the coastal flow) and melting reduces its density sufficiently to allow it to escape Filchner Depression between 32°W and 34°W.

[18] With its limited resolution the model is unable to resolve tidal rectification, which generates residual currents that exchange 0.35 Sv across the ice fronts and drive a 0.1-Sv flow around Berkner Island [*Makinson and Nicholls*, 1999]. Tidal mixing fronts and the significant associated flows that drive water masses across the ice front and within the cavity [*Nicholls et al.*, 2004] also remain unresolved. This study will therefore underestimate the influence of tides beneath FRIS, with net melting and the fluxes through the cavity and at the overflow being even greater than predicted here.

5. Conclusions

[19] We have studied the effect of including tidal forcing in a numerical simulation of the interaction between FRIS and the southern Weddell Sea. Inclusion of tides causes the net flux through the cavity and the net basal melting to almost double to 0.58 Sv and 0.22 m a^{-1}, with the enhanced net flux and internal recirculation, or ice pump, increasing melting 3-fold and refreezing 6-fold, effectively moving vast volumes of ice around the sub-ice shelf cavity. With tides, the modeled net melt is close to glaciological estimates, and the model shows reasonable skill at reproducing both the spatial pattern and magnitude of basal melting and freezing, important to ice shelf morphology. In addition, it reproduces the major outflow of ISW over Filchner Sill, which ultimately contributes to the bottom water inventory. Our results clearly demonstrate that, in the tidally-energetic Weddell Sea sector at least, the inclusion of tidal forcing within ocean models is critical to understanding ice shelf-ocean interactions and deep water formation.

[20] **Acknowledgments.** The authors and editor thank two anonymous reviewers.

References

Bleck, R., C. Rooth, D. Hu, and L. T. Smith (1992), Salinity-driven thermocline transients in a wind- and thermohaline-forced isopycnic model of the North Atlantic, *J. Phys. Oceanogr.*, *22*, 1486–1505, doi:10.1175/1520-0485(1992)022<1486:SDTTIA>2.0.CO;2.

Foldvik, A., T. Gammelsrød, E. Nygaard, and S. Østerhus (2001), Current meter measurements near Ronne Ice Shelf, Weddell Sea: Implications for circulation and melting underneath the Filchner-Ronne ice shelves, *J. Geophys. Res.*, *106*(C3), 4463–4477, doi:10.1029/2000JC000217.

Foldvik, A., T. Gammelsrød, S. Østerhus, E. Fahrbach, G. Rohardt, M. Schröder, K. W. Nicholls, L. Padman, and R. A. Woodgate (2004), Ice shelf water overflow and bottom water formation in the southern Weddell Sea, *J. Geophys. Res.*, *109*, C02015, doi:10.1029/2003JC002008.

Gammelsrød, T., A. Foldvik, O. A. Nøst, Ø. Skagseth, L. G. Anderson, E. Fogelqvist, K. Olsson, T. Tanhua, E. P. Jones, and S. Østerhus (1994), Distribution of water masses on the continental shelf in the southern Weddell Sea, in *The Polar Oceans and Their Role in Shaping the Global Environment*, *Geophys. Monogr. Ser.*, vol. 85, edited by O. M. Johannesen, R. D. Muench, and J. E. Overland, pp. 159–176, AGU, Washington, D. C.

Holland, D. M., and A. Jenkins (2001), Adaptation of an isopycnic coordinate ocean model for the study of circulation beneath ice shelves, *Mon. Weather Rev.*, *129*(8), 1905–1927, doi:10.1175/1520-0493(2001)129<1905:AOAICO>2.0.CO;2.

Holland, P. R., D. L. Feltham, and A. Jenkins (2007), Ice shelf water plume flow beneath Filchner-Ronne Ice Shelf, Antarctica, *J. Geophys. Res.*, *112*, C05044, doi:10.1029/2006JC003915.

Jenkins, A., and D. M. Holland (2002), A model study of ocean circulation beneath Filchner-Ronne Ice Shelf, Antarctica: Implications for bottom water formation, *Geophys. Res. Lett.*, *29*(8), 1193, doi:10.1029/2001GL014589.

Jenkins, A., D. M. Holland, K. W. Nicholls, M. Schröder, and S. Østerhus (2004), Seasonal ventilation of the cavity beneath Filchner-Ronne Ice Shelf simulated with an isopycnic coordinate ocean model, *J. Geophys. Res.*, *109*, C01024, doi:10.1029/2001JC001086.

Joughin, I., and L. Padman (2003), Melting and freezing beneath Filchner-Ronne Ice Shelf, Antarctica, *Geophys. Res. Lett.*, *30*(9), 1477, doi:10.1029/2003GL016941.

Lambrecht, A., H. Sandhager, D. G. Vaughan, and C. Mayer (2007), New ice thickness maps of Filchner-Ronne Ice Shelf, Antarctica, with specific focus on grounding lines and marine ice, *Antarct. Sci.*, *19*(4), 521–532, doi:10.1017/S0954102007000661.

Larour, E., E. Rignot, I. Joughin, and D. Aubry (2005), Rheology of the Ronne Ice Shelf, Antarctica, inferred from satellite radar interferometry data using an inverse control method, *Geophys. Res. Lett.*, *32*, L05503, doi:10.1029/2004GL021693.

Lewis, E. L., and R. G. Perkin (1986), Ice pumps and their rates, *J. Geophys. Res.*, *91*(C10), 11,756–11,762, doi:10.1029/JC091iC10p11756.

Lythe, M. B., and D. G. Vaughan (2001), BEDMAP: A new ice thickness and subglacial topographic model of Antarctica, *J. Geophys. Res.*, *106*(B6), 11,335–11,351, doi:10.1029/2000JB900449.

MacAyeal, D. R. (1984), Thermohaline circulation below the Ross Ice Shelf: A consequence of tidally induced vertical mixing and basal melting, *J. Geophys. Res.*, *89*(C1), 597–606, doi:10.1029/JC089iC01p00597.

Makinson, K., and K. W. Nicholls (1999), Modeling tidal currents beneath Filchner-Ronne Ice Shelf and on the adjacent continental shelf: their effect on mixing and transport, *J. Geophys. Res.*, *104*(C6) 13,449–13,465, doi:10.1029/1999JC900008.

Nicholls, K. W., and K. Makinson (1998), Ocean circulation beneath the western Ronne Ice Shelf, as derived from in situ measurements of water currents and properties, in *Ocean, Ice, and Atmosphere: Interactions at the Antarctic Continental Margin*, *Antarct. Res. Ser.*, vol. 75, edited by S. S. Jacobs and R. F. Weiss, pp. 301–318, AGU, Washington, D. C.

Nicholls, K. W., L. Padman, M. Schröder, R. A. Woodgate, A. Jenkins, and S. Østerhus (2003), Water mass modification over the continental shelf north of Ronne Ice Shelf, Antarctica, *J. Geophys. Res.*, *108*(C8), 3260, doi:10.1029/2002JC001713.

Nicholls, K. W., K. Makinson, and S. Østerhus (2004), Circulation and water masses beneath the northern Ronne Ice Shelf, Antarctica, *J. Geophys. Res.*, *109*, C12017, doi:10.1029/2004JC002302.

Nicholls, K. W., L. Boehme, M. Biuw, and M. A. Fedak (2008), Wintertime ocean conditions over the southern Weddell Sea continental shelf, Antarctica, *Geophys. Res. Lett.*, *35*, L21605, doi:10.1029/2008GL035742.

Nicholls, K. W., S. Østerhus, K. Makinson, T. Gammelsrød, and E. Fahrbach (2009), Ice-ocean processes over the continental shelf of the southern Weddell Sea, Antarctica: A review, *Rev. Geophys.*, *47*, RG3003, doi:10.1029/2007RG000250.

Olbers, D. J., V. Gouretski, G. Seiβ, and J. Schröter (1992), *Hydrographic Atlas of the Southern Ocean*, Alfred Wegener Inst., Bremerhaven, Germany.

Padman, L., H. A. Fricker, R. Coleman, S. Howard, and L. Erofeeva (2002), A new tide model for the Antarctic ice shelves and seas, *Ann. Glaciol.*, *34*, 247–254, doi:10.3189/172756402781817752.

Robertson, R. (2005), Baroclinic and barotropic tides in the Weddell Sea, *Antarct. Sci.*, *17*(3), 461–474, doi:10.1017/S0954102005002890.

Timmermann, R., H. H. Hellmer, and A. Beckmann (2002), Simulations of ice-ocean dynamics in the Weddell Sea: 2. Interannual variability 1985–1993, *J. Geophys. Res.*, *107*(C3), 3025, doi:10.1029/2000JC000742.

D. M. Holland, Courant Institute of Mathematical Sciences, New York University, 251 Mercer St., New York, NY 10012, USA.

P. R. Holland, A. Jenkins, K. Makinson, and K. W. Nicholls, British Antarctic Survey, High Cross, Madingley Road, Cambridge CB3 0ET, UK. (kmak@bas.ac.uk)